Chemical Process Design Vol.2 No.2 (2023) 52-59

University of Sistan and Baluchestan

Chemical Process Design

Available online at http://cpd.usb.ac.ir/



Synthesis of Hematite Nanoparticles by Milling Process and the Study of the Magnetic Properties and its Microstructure

Esmaeil Koohestanian*, Somayeh Mehdigholami

Department of Chemical Engineering, Iranshahr Branch, Islamic Azad University, Iranshahr, Iran

ARTICLE INFO

Article history:
Received: 2023-12-05
Received in revised form: 2023-12-29
Accepted: 2023-12-31
Published online: 2023-12-31

Keywords:
Nanoparticles;
Hematite;
Ball milling process;
Superparamagnetic

DOI: *10.22111/CPD.2024.47291.1030*

ABSTRACT

This study focuses on synthesizing and characterizing hematite nanoparticles using the ball milling process. The research investigates the changes in microstructure and magnetic properties of the powders during the milling process using XRD, SEM, TEM, and VSM techniques. The crystallite size is determined through XRD patterns using Scherer methods. It is found that the particle size decreases and lattice parameters with extended milling times. XRD and TEM analysis estimates the average particle size of the hematite nanoparticles to be around 30 nm and 12 nm, respectively. The SEM image shows uniform dispersion and spherical morphology. The magnetic saturation increases as a result of the ball milling process, and the VSM results indicate that the saturation magnetic value increases with longer milling times. The morphology of the particles is predominantly spherical or semi-spherical. The study concludes that the shape and size of the synthesized particles are influenced by the milling time parameter. Both SEM and XRD results highlight the significant influence of milling time on the shape and size of the synthesized particles.

1. Introduction

Mechanical ball milling (BM) is a cost-effective powder processing technique that involves the deformation, fracturing, and cold welding of particles during repeated collisions with balls in a high-energy milling environment. It is used to synthesize a variety of non-equilibrium and equilibrium materials [1]. This method provides a simple and inexpensive processing route for producing materials in large quantities and at a low cost [2].

In recent years, BM has been widely used to produce new magnetic materials, including ferrites, rare-earth permanent magnets, and ultrafine powders [3]. Hematite nanoparticles (α-Fe_2O_3) have gained significant attention in

Corresponding author. Tel.: +98-54-3722-1036; fax: +98-54-3722-1036.
E-mail address: koohestanian@pgs.usb.ac.ir (E. Koohestanian)

nanotechnology due to their unique characteristics such as availability, low cost, abundance, high saturation fields, and enhanced anisotropy contributions resulting from finite size and high surface area effects [4-6]. This makes hematite (α-Fe_2O_3) not only a strategic material for industry but also one of the most versatile metal oxides, finding applications in fields such as magnetism, electrochemistry, catalysis, and biotechnology [7]. For example, it is commonly used as a catalyst in the chemical industry [8] and can be applied in biomedical applications such as laboratory diagnostics and drug delivery systems [9]. Wet ball milling involves the use of a liquid medium during the milling process, which can contribute to the formation of nanoparticles with unique properties. Studying the structural characteristics allows for understanding the physical and chemical properties of these nanoparticles, along with their potential applications in fields like catalysis, electronics, and medicine. The synthesis of hematite nanoparticles through wet ball milling provides a cost-effective and scalable method for producing these nanomaterials.

This paper focuses on investigating the structural characteristics of hematite nanoparticles synthesized using wet ball milling at room temperature with methanol as the organic carrier liquid. The synthesized nanoparticles are characterized using chemical analysis such as; scanning electron microscopy (SEM), transmission electron microscopy (TEM), and X-ray diffraction (XRD). The magnetic properties are measured using a vibrating sample magnetometer (VSM). The crystallite size is determined through XRD patterns using Scherrer methods. The study explores the effects of milling time, the weight ratio of methanol to powder (R), and the precipitation time of the solution containing the synthesized nanoparticles on the particle size.

2. Experimental

2.1. Experimental setup

In the experiment, nine samples were prepared using a Fritsch Pulverisette 5 planetary ball mill. Each sample contained hematite (α-Fe_2O_3) particles dispersed in methyl alcohol (CH_3OH) as the carrier liquid. A mixture of hematite powder (99.99% purity, mean particle size of 5 μm) and methyl alcohol was charged into a hardened steel vial with a volume of 60 cc. The vial was charged in a glove box filled with argon to minimize contaminants during milling and sealed with an O-ring. Ball milling processes were carried out at a speed of 300 rpm, and different milling durations of 10, 30, and 60 hours. To prevent excessive temperature, increase within the vial, a 60-minute milling period was followed by a 10-minute cooling interval.

2.2. Characterization of microstructure

XRD measurements were performed using a D8 Advance with Cu-kα radiation (λ=1.5418Å) in the 2θ range from 20 to 80˚. X-ray diffraction line broadening is influenced by the crystallite size. XRD measurements were conducted using a D8 Advance instrument with Cu-kα radiation, where the wavelength of the radiation (λ) was 1.5418Å. The measurements were performed in the 2θ range from 20 to 80˚. It is known that the broadening of XRD lines is affected by the size of the crystallites [10]. The equation used to determine crystallite size (D) based on XRD line broadening is: [11]:

$$D = \frac{k.\lambda}{\beta.\cos\theta} \tag{1}$$

In this equation, "k" is a constant which is typically assumed to be 0.9, λ represents the Cu Kα radiation wavelength, θ is half the diffraction angle, and β is the full-width at half maximum intensity, given in radians.

The morphology of the particles was investigated using a kyky-EM3200 SEM operated at an accelerating voltage of 25 kV. Before SEM observation, the samples were coated with a thin layer of gold using a sputtering process to enhance conductivity and image quality. Magnetic properties were evaluated using a VSM. The hysteresis loop was measured to assess the magnetic behavior of the samples. Additionally, the isothermal remanence magnetization (IRM) curve and direct current demagnetization (DCD) remanence curve were measured to further understand the magnetization properties of the samples.

3. Results and discussion

3.1. The structural and morphological characteristics of nanoparticles

The XRD patterns are shown in Fig. 1 for both the raw powders and powders in the milling vessel during different milling conditions. All Bragg peaks of the XRD patterns showed only the hematite reflections, indicating that there are no phase changes during the milling [12]. An analysis of the XRD results shows that there is broadening, shifting, and a reduction in peak intensity as the duration of ball milling increases. This broadening of peaks indicates that the grain size is being reduced during the milling process. Initially, in the early step of BM, the reduction in grain size is rapid. However, as the milling time increases, the rate of reduction gradually slows down. When the BM time is increased, the peaks become broader, indicating that the grain size becomes smaller. As the grain size decreases, the number of grain boundaries increases. Consequently, the ratio of area to volume also increases, leading to an increase in the number of atoms at the surface. As a result, the number of free bonds in the atoms increases, causing the average force per atom from adjacent atoms to decrease. This leads to an increase in lattice strain within the smaller grains, ultimately affecting the lattice parameter and peak broadening observed in the XRD pattern.

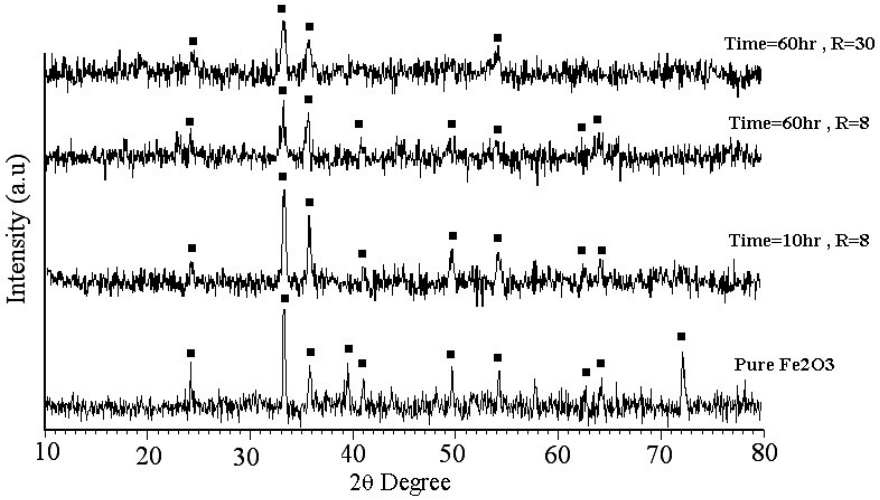


Fig. 1. XRD patterns of the powders, milled for various conditions at fixed milling speed (300 rpm)

The results reveal that the crystallite size of hematite is decreased with milling time and R by this method. The crystallite size of the prepared sample (milled for 60 hr and R=30) was obtained at about 30 nm by Sherrer's method. In addition, we observed an increase in the lattice parameters with increasing milling time. In summary, by increasing of milling time, the diffraction peaks become broader and their relative intensity decreases, thus the grain size is decreased and the lattice strain increased. All these results summarized in Table 1 are in good agreement with previously reported results [12, 13].

Table 1. Lattice parameter and crystallite size of synthesis nanoparticles in different BM conditions

Milling time (hr)	Raw powder	10	60	60
R	-	8	8	30
Crystallite size	5µm	40 nm	30 nm	30 nm
Lattice parameter (%)	0.259	0.302	0.400	0.401

SEM micrographs of the samples before and after milling are shown in Fig. 2. It is clear that unmilled powder (Fig. 2a) shows in homogeneities regarding particle size distribution. After milling, a reduction of the particle size can be observed with relatively better homogeneity.

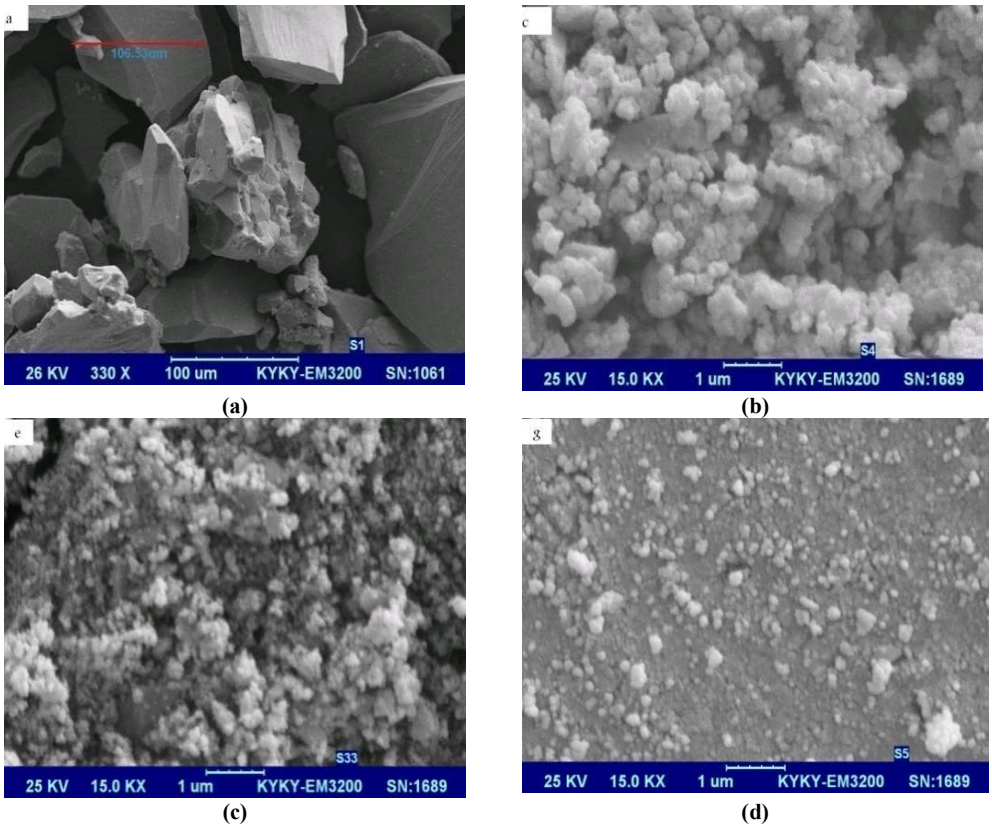


Fig. 2. SEM images of α-Fe_2O_3 powder for R=15 and different milling times: (a) as received; (b) milled for 10 hr; (c) milled for 30 hr; and (d) milled for 60 hr

In these figures (Fig. 2(b) to Fig. 2(d)), fine sub-rounded α-Fe_2O_3 particles with narrow particle size distribution are observed. With increased milling time, a considerable decrease in particle size is apparent due to both the increased number of ball collisions and increased energy from the balls during wet ball milling. The morphology of these particles is spherical or semi-spherical. Due to the high surface-to-volume ratio in spherical shape, it is the best morphology for different applications.

Fig. 3, TEM image shows nanoparticles (α-Fe_2O_3). As it is determined by the figure, the hematite nanoparticles have spherical morphology. The average of the synthesized hematite nanoparticles was obtained at 12nm.

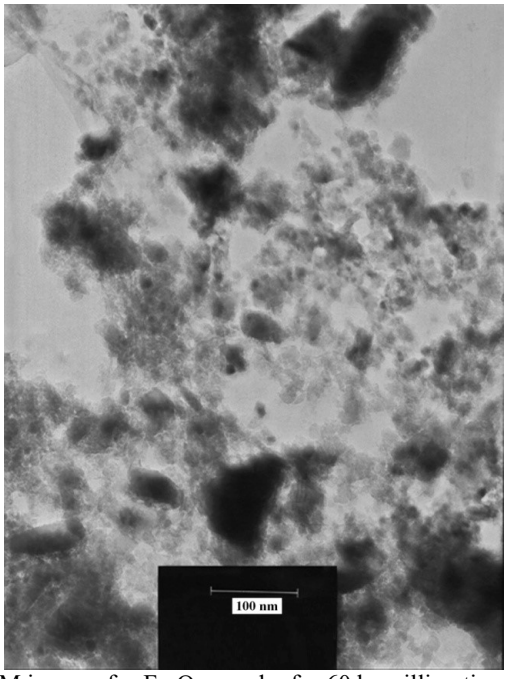


Fig. 3. TEM image of α-Fe_2O_3 powder for 60 hr milling time and R=30

The reason for particle difference in TEM and SEM is that preparation was performed by ultrasonic device in TEM, and particles were separated, thus the irregular shape which was observed in SEM will be eliminated by ultrasonic device then particle shapes will be reported suitably.

3.2. Magnetic properties

Diminution in magneto-crystalline anisotropy due to smaller average crystallite size, leads to an easier rotation of the magnetic vector. When the grain size is larger than the magnetic exchange length L_{ex}, the coercivity depends on the crystallite size and the magnetization saturation as [14]:

$$H_C \approx 3\sqrt{\frac{kT_C K_1}{aM_S}}\frac{1}{D} \tag{2}$$

where H_C is the coercivity, D is the crystallite size, M_S is the saturation magnetization, K_1 is the magneto-crystalline anisotropy, T_C is the Curie temperature, k is the Boltzmann constant and a is the lattice constant. L_{ex} can be expressed as [15]:

$$L_{ex} = \sqrt{\frac{A}{K_1}} \tag{3}$$

where A is the exchange stiffness constant. At the grain sizes above L_{ex} the grain boundaries result in the pinning of the domain walls [16]. Increasing the volume fraction of grain boundaries through grain refinement impedes the domain walls movement, thereby increasing the coercivity [17]. On the other hand, when the grain size is smaller than the magnetic exchange length, the domain wall effect diminishes and each grain behaves as a single domain [18]. Based on the random anisotropy model, the coercivity can be expressed as [19, 20]:

$$H_C = \frac{P_C K_1^4 D^6}{\mu_0 M_S A^3} \tag{4}$$

where P_C is a constant of the order of unity, and μ_0 is the permeability of free space.

Fig. 4 shows the hysteresis curve for hematite powder in different conditions BM and 8500Oe applied field. By noticing to figure, the saturation magnetizing ratio will be increased by increasing BM time. Also, the H_C will be decreased because of micro grains effect (random anisotropy model) by increasing of BM time to 60hr. The transformation of this curve with increasing BM time shows the dependence of magnetic properties on microstructure. The rate of magnetic fields was decreased in each particle into nano structural by comparing the microstructural and thus, the interaction of magnetic moments among atoms and their magnetic effectiveness will be increased and exchangeable interaction among magnetic fields will be decreased and the material is magnetized with low energy [21]. Generally, different factors that affect avoidably the coercive force in BM are followed: internal micro strains, grossness, cavities, and faults which were obtained avoidably during the BM process. These can increase demagnetizing force which is one of the magnetic properties sensitive to microstructure [22]. But in this step, the effect of micro grains which is explainable by the random anisotropy model is a predominant mechanism. According Herzer model, when grain size is smaller their magnetic exchange length (L_{ex}), a direct relation with grain size from 6 degrees (eq. 4) and so the coercive force will be decreased by decreasing of grain size which is an advantage of nanocrystal and amorphous. The crystals that have oriented randomly don't resist Bloch wall motions and coercivity will be decreased [23]. The size of synthesized nanoparticles will be decreased by increasing BM time.

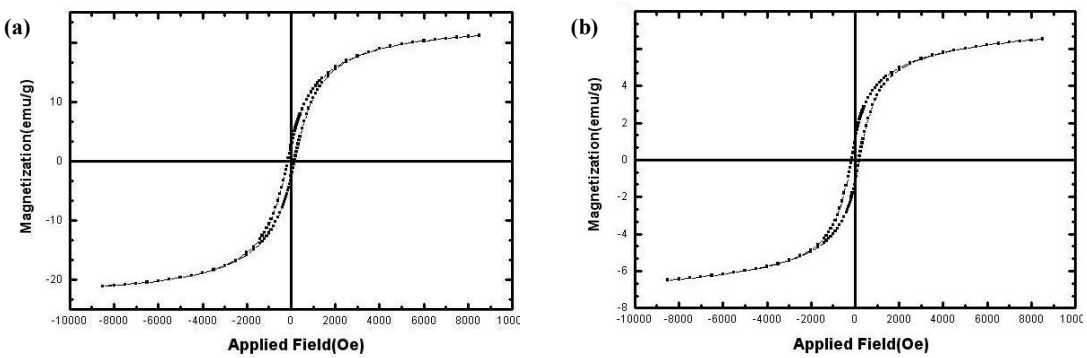


Fig. 4. Hysteresis loops of α-Fe_2O_3 powder at: (a) 10 hr milling time and R=8; (b) 60 hr milling time and R=30

4. Conclusion

The wet ball milling procedure is a low-cost method to produce a mass of nanoparticles, because of both cold welding and fracturing, the final product has a wide range of distribution (from nanometer to micrometer) which is a basic defect of ball milling. However, this research reached more uniform particles in a limited range and selective distribution by using wet ball milling and giving optimum precipitation time for the separation of various phases of synthesized nanoparticles with different sizes. Furthermore, another ball milling problem is the pollution of powder because of mill grind components (ball and vial mill). However, because ball milling was performed in a wet medium, friction between mill grind components and the vial mill was decreased. Also, because of the desirability of the vial and used balls, there weren't any in XRD results hence this research can meet one of the other faults from synthesis matters by helping ball milling by considering special plans. Also, XRD analysis results confirm that wet ball milling of hematite micrometric powder processing can be used to synthesize hematite nanoparticles without oxidation and phase transformation. However, XRD and TEM estimated the average particle size of the hematite nanoparticles as about 30 and 12 nm, respectively which put them into the category of superparamagnetic iron oxide ultrafine particles whose diameter is less than 50 nm. Also, the result of VSM shows that saturation magnetic will be increased as a

result of ball milling time. The morphology of this particle was spherical or semi-spherical. Results of SEM and XRD show that the influence of the milling time parameter is greater than other parameters in the shape and size of synthesis particles.

Nomenclature

a	Lattice constant
A	Exchange stiffness constant
D	Crystallite size
H_C	Coercivity
K	Boltzmann constant
K_1	Magneto-crystalline anisotropy
L_{ex}	Magnetic exchange length
M_S	Saturation magnetization
P_C	Constant of the order of unity
R	Methanol to hematite powder
T_C	Curie temperature
Abbreviation	
BM	Ball Milling
BPR	Balls to Powder Ratio
DCD	Direct Current Demagnetization
IRM	Isothermal Remanence Magnetization
SEM	Scanning Electron Microscope
TEM	Transmission Electron Microscopy
VSM	Vibrating Sample Magnetometer
XRD	X-Ray Diffraction
Greek letters	
β	The full-width at half maximum intensity
λ	Cu Kα radiation wavelength (λ=1.5418Å)
θ	Half the diffraction angle
μ_0	Permeability of free space

References

[1] Bidarian, V., Koohestanian, E., Omidvar, M., 2017. Dynamic modeling of hardness changes of aluminum nanostructure during the mechanical ball milling process, Journal of Particle Science and Technology, 3(1), 25-32. https://doi.org/10.22104/JPST.2017.1527.1047

[2] Omidvar, M., Koohestanian, E., Ramezani-Azghandi, O., 2016. Synthesis and Statistical Analysis of Changing Size of Nano-structured PbO_2 during Mechanical Milling Using Taguchi Methodology, Journal of Particle Science & Technology, 2(1), 49-54. https://doi.org/10.22104/JPST.2016.391

[3] Aslibeiki, B., Kameli, P., 2020. Structural and magnetic properties of Co/Al_2O_3 cermet synthesized by mechanical ball milling, Ceramics International, 46(12), 20116-20121. https://doi.org/10.1016/j.ceramint.2020.05.086

[4] Basavegowda, N., Mishra, K., Lee, Y.R., 2017. Synthesis, characterization, and catalytic applications of hematite (α-Fe_2O_3) nanoparticles as reusable nanocatalyst, Advances in Natural Sciences: Nanoscience and Nanotechnology, 8(2), 025017. https://doi.org/10.1088/2043-6254/aa6885

[5] Kefeni, K.K., Msagati, T.A.M., Nkambule, T.T.I., Mamba, B.B., 2018. Synthesis and application of hematite nanoparticles for acid mine drainage treatment, Journal of Environmental Chemical Engineering, 6(2), 1865-1874. https://doi.org/10.1016/j.jece.2018.02.037

[6] Rufus, A., Sreeju, N., Philip, D., 2016. Synthesis of biogenic hematite (α-Fe_2O_3) nanoparticles for antibacterial and nanofluid applications, RSC advances, 6(96), 94206-94217. https://doi.org/10.1039/C6RA20240C

[7] Al-Hakkani, M.F., Gouda, G.A., Hassan, S.H., 2021. A review of green methods for phyto-fabrication of hematite (α-Fe_2O_3) nanoparticles and their characterization, properties, and applications, Heliyon, 7(1). https://doi.org/10.1016/j.heliyon.2020.e05806

[8] Fouad, D.E., Zhang, C., Mekuria, T., Bi, D., Zaidi C., Shah A.H., 2019. Effects of sono-assisted modified precipitation on the crystallinity, size, morphology, and catalytic applications of hematite (α-Fe_2O_3) nanoparticles: A comparative study, Ultrasonics sonochemistry, 59, 104713. https://doi.org/10.1016/j.ultsonch.2019.104713

[9] Gerami, S.E., Pourmadadi, M., Fatoorehchi H., Yazdian, F., Rashedi, H., Nigjeh, M.N., 2021. Preparation of pH-sensitive chitosan/polyvinylpyrrolidone/α-Fe_2O_3 nanocomposite for drug delivery application: Emphasis on ameliorating restrictions, International Journal of Biological Macromolecules, 173, 409-420. https://doi.org/10.1016/j.ijbiomac.2021.01.067

[10] Mehdigholami, S., Koohestanian, E., 2023. Fe_3O_4@ SiO_2/AEPTMS/Fe(OTf)3: An efficient superparamagnetic nanocatalyst for the protecting of alcohols. Journal of Particle Science and Technology, 9(1), 1-9. https://doi.org/10.22104/JPST.2023.6188.1224

[11] Nasiri, S., Rabiei, M., Palevicius, A., Janusas, G., Vilkauskas, A., Nutalapati, V., Monshi, A., 2023. Modified Scherrer equation to calculate crystal size by XRD with high accuracy, examples Fe_2O_3, TiO_2 and V_2O_5, Nano Trends, 3, 100015. https://doi.org/10.1016/j.nwnano.2023.100015

[12] Pourghahramani, P., Altin, E., Mallembakam, M.R., Peukert, W., Forssberg, E., 2008. Microstructural characterization of hematite during wet and dry millings using Rietveld and XRD line profile analyses, Powder Technology, 186(1), 9-21. https://doi.org/10.1016/j.powtec.2007.10.027

[13] Lemine, O., 2009. Microstructural characterisation of nanoparticles using, XRD line profiles analysis, FE-SEM and FT-IR, Superlattices and Microstructures, 45(6), 576-582. https://doi.org/10.1016/j.spmi.2009.02.004

[14] Sourmail, T., 2005. Near equiatomic FeCo alloys: Constitution, mechanical and magnetic properties, Progress in Materials Science, 50(7), 816-880. https://doi.org/10.1016/j.pmatsci.2005.04.001

[15] McHenry, M.E., Willard, M.A., Laughlin, D.E., 1999. Amorphous and nanocrystalline materials for applications as soft magnets, Progress in Materials Science, 44(4), 291-433. https://doi.org/10.1016/S0079-6425(99)00002-X

[16] Simões, A., Cavalcante, L.S., Moura, F., Longo, E., Varela, J.A., 2011. Structure, ferroelectric/magnetoelectric properties and leakage current density of $(Bi_{0.85}Nd_{0.15})FeO_3$ thin films, Journal of Alloys and Compounds, 509(17): p. 5326-5335. https://doi.org/10.1016/j.jallcom.2011.02.030
[17] Tang, X., Sepehri-Amin, H., Ohkubo T., Hono, H., 2018. Suppression of non-oriented grains in Nd-Fe-B hot-deformed magnets by Nb doping, Scripta Materialia, 147, 108-113. https://doi.org/10.1016/j.scriptamat.2017.12.032
[18] Nagy, L., Williams, W., Tauxe, L., Muxworthy, A.R., 2019. From nano to micro: Evolution of magnetic domain structures in multidomain magnetite, Geochemistry, Geophysics, Geosystems, 20(6), 2907-2918. https://doi.org/10.1029/2019GC008319
[19] Herzer, G., 1990. Grain size dependence of coercivity and permeability in nanocrystalline ferromagnets, Magnetics, IEEE Transactions on Magnetics, 26(5), 1397-1402. https://doi.org/10.1109/20.104389
[20] Comstock, R.L., Comstock, L.R., 1999. Introduction to magnetism and magnetic recording, 2nd Edition, Published by John Wiley, 487 pages.
[21] Cullity, B., Graham, C., 1972. Introduction to Magnetic Materials, 2nd Edition, Published by IEEE Press, MA: Addison-Wesley, 544 pages.
[22] Lee, B.H., Ahn, B.S., Kim, D.G., Oh, S.T., Jeon, H., Ahn, J., Kim, Y.D., 2003. Microstructure and magnetic properties of nanosized Fe–Co alloy powders synthesized by mechanochemical and mechanical alloying process, Materials Letters, 57(5), 1103-1107. https://doi.org/10.1016/S0167-577X(02)00938-2
[23] Schöbitz, M., 2021. Current-induced magnetic Bloch-point domain wall dynamics in cylindrical nanowires, Ph.D. thesis Department of Physic, Friedrich-Alexander-Universität (FAU), Erlangen-Nürnberg, Germany.